Optimization of compensation for high spatial frequency in distorted wavefront using optical phase conjugation

Pan Zhang (张 盼)[1,2], Dean Liu (刘德安)[1,*], Aihua Yang (杨爱华)[1,2], and Jianqiang Zhu (朱健强)[1]

[1]*Key Laboratory of High Power Laser and Physics, Shanghai Institute of Optics and Fine Mechanics, Chinese Academy of Sciences, Shanghai 201800, China*

[2]*Center of Materials Science and Optoelectronics Engineering, University of Chinese Academy of Sciences, Beijing 100049, China*

**Corresponding author: liudean@siom.ac.cn*

Received October 22, 2018; accepted April 12, 2019; posted online July 1, 2019

A method is proposed to optimize the recording structure of the photorefractive volume grating to compensate high spatial frequency in the distorted wavefront by optical phase conjugation. Based on the coupled-wave equation, the diffraction efficiency of the recorded grating formed by the scattered beams in different recording structures is simulated. The theoretical results show that the recorded modulations with high spatial frequency can be significantly improved in the small recording angle. In the experiment, three recording structures with the recording angles of 7.5°, 30°, and 45° are chosen to verify the compensation effect. Compared with the reconstructed image in the large recording angle of 45°, the signal to noise ratio of the image recorded at 7.5° increases to 3.2 times of that at 45°.

OCIS codes: 090.7330, 110.0113, 070.5040.
doi: 10.3788/COL201917.070901.

Imaging through scattering media is one of the most challenging problems in optics. The extensive scattering of light by scattering media is a significant obstacle for imaging and focusing. Suppression of the scattering effect can be realized by modulating the shape of the wavefront by transmission matrix measurement[1–3], iterative wavefront optimization[4,5], and optical phase conjugation (OPC)[6–9]. Among them, OPC[10] with its time-reversal nature determines the optimum wavefront without time-consuming iterations. Generally, OPC can be generated by adaptive optics, named digital OPC (DOPC)[11]. In addition, OPC is also achieved by using the analog OPC technique[12–14] based on volume grating in the photorefractive crystals[15,16], which can inherently compensate the distorted wavefront. In contrast to DOPC, analog OPC is more convenient for achieving conjugating phase without inversion and the fine adjustments of relative phase differences.

In principle, the analog OPC based on volume grating of the photorefractive crystals can be the proper way to compensate the distortion effectively. However, the modulations with high spatial frequency in the wavefront are always introduced by scattering media. Limited by the recording structure of the photorefractive volume grating, the diffraction efficiency of the high-frequency modulations in the distorted wavefront is weak, and the compensation effect of wavefront distortion is greatly reduced. In photorefractive crystals, the effective wave vector of the photorefractive grating is determined by the angle between the vector direction of the volume grating and the optical axis direction of the photorefractive crystal[17–19]. Taking into account the above problems in analog OPC, optimization of the recording structure to obtain a high-quality compensation effect with high signal to noise ratio (SNR) is worthy of study.

In this Letter, we optimize the volume grating structure in analog OPC generated by the photorefractive $LiNbO_3$ crystal. The compensation effect for the high spatial frequency in the distorted wavefront is theoretically analyzed and experimentally verified. Based on the couple-wave equation of volume grating, we theoretically analyze the effective wave vector ratio of high spatial frequency in the distorted wavefront and the diffraction efficiency of the signal volume grating with the recording angle. In the experiment, the analog OPC system based on the photorefractive grating is constructed to verify the compensation effects of the distorted wavefront with the recording angle θ at 7.5°, 30°, and 45°, respectively. Combining the theoretical analysis and the experimental results, the SNR of the compensated images by the OPC with different recording angles is further analyzed, and the optimal recording structure of the photorefractive volume grating is concluded.

Analyses for optimizing the structure of the photorefractive volume grating are focused on two steps: the recording and reconstructing of the distorted wavefront by the photorefractive volume grating. In the recording process, the geometry structure of the photorefractive volume grating is depicted in Fig. 1. The electro-optic axis $\hat{c}$ is oriented along the z direction. The bisector of the angle between the two recording beams is parallel to the x direction. The reference beam $\boldsymbol{E}_r$ intersects with signal beam $\boldsymbol{E}_o$, and the complex field amplitudes can be written as

$$\begin{aligned}\boldsymbol{E}_r(x,z) &= \boldsymbol{A}(x,z)\exp(-i\boldsymbol{k}_r r),\\ \boldsymbol{E}_o(x,z) &= \boldsymbol{a}(x,z)\exp(-i\boldsymbol{k}_o r),\end{aligned} \tag{1}$$

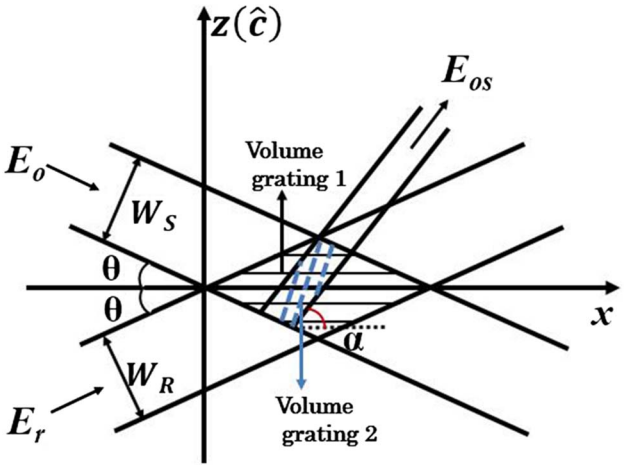

Fig. 1. Recording geometry of scattered beams by photorefractive volume grating. Volume gratings 1 and 2 represent the signal volume grating and the photorefractive volume grating with high spatial frequency. $\boldsymbol{E}_r$, $\boldsymbol{E}_o$, and $\boldsymbol{E}_{\rm os}$ represent the reference beam, signal beam, and scattered noise beam, respectively. θ is the recording angle, W_R and W_S are the widths of $\boldsymbol{E}_r$ and $\boldsymbol{E}_o$, respectively. α is the angle between $\boldsymbol{E}_{\rm os}$ and the x axis.

where $\boldsymbol{A}$, $\boldsymbol{a}$ and $\boldsymbol{k}_r$, $\boldsymbol{k}_o$ represent the complex amplitude and the wave vector of $\boldsymbol{E}_r$ and $\boldsymbol{E}_o$, respectively. The wave vector $\boldsymbol{k}$ of the signal volume grating formed by the two waves parallel to the z direction in the crystal can be expressed as

$$\boldsymbol{k} = \boldsymbol{k}_r - \boldsymbol{k}_o, \tag{2}$$

as the distortion generated by the scattering medium is introduced in the signal wave. For the recording information of the distorted wavefront, the original signal information can be regarded as the low spatial frequency component. Correspondingly, the scattered noise information can be considered as the high spatial frequency component. A scattered noise beam $\boldsymbol{E}_{\rm os}$ is supposed, with the angle α relative to the x axis, and the complex field amplitude can be written as

$$\boldsymbol{E}_{\rm os}(x,z) = \boldsymbol{B}(x,z)\exp(-i\boldsymbol{k}_{\rm os}r), \tag{3}$$

where $\boldsymbol{B}$ and $\boldsymbol{k}_{\rm os}$ are the complex amplitude and the wave vector of $\boldsymbol{E}_{\rm os}$, respectively. The wave vector $\boldsymbol{k}_s$ of the photorefractive volume grating with high spatial frequency formed by $\boldsymbol{E}_{\rm os}$ and $\boldsymbol{E}_r$ is $\boldsymbol{k}_s = \boldsymbol{k}_r - \boldsymbol{k}_{\rm os}$. $\boldsymbol{k}'_s$ is defined as the component of wave vector $\boldsymbol{k}_s$ parallel to the c axis in the crystal; it can be written as

$$\boldsymbol{k}'_s = \boldsymbol{k}_s\cos[(\alpha+\theta)/2]. \tag{4}$$

The recorded information of the photorefractive volume grating with high spatial frequency is a component of the scattered noise information because of the recording intensity determined by the wave vector. Thus, in order to obtain a clear physical description about this grating, we define the effective wave vector ratio as $\frac{k'_s}{k_s} = \cos[(\alpha+\theta)/2]$, which represents the recorded modulations with high spatial frequency parallel to the z direction.

Due to the photorefractive effect, the signal volume grating with the modulation n_1 is formed by $\boldsymbol{E}_r$ and $\boldsymbol{E}_o$ in the crystal. The wave number is $k = \pi n_1/\lambda$, where λ is the wavelength of the recording waves. n_1, the refractive index modulation in the photorefractive crystal, is assumed constant with $n_1 = 0.15\times10^{-4}$. The recorded intensity and diffraction efficiency[19] of the signal volume grating are determined by the recording structures. Similarly, the photorefractive volume grating with high spatial frequency is also recorded in the same way.

To analyze the diffraction behavior of the signal volume grating and photorefractive volume grating with high spatial frequency during the conjugate reconstruction, we take the signal volume grating as an example due to the similar physical mechanism. In the conjugate reconstruction process, the wave field in the signal volume grating can be written as

$$\boldsymbol{E}(x,z) = \boldsymbol{a}^*(x,z)e^{ik_o r} + \boldsymbol{Q}(x,z)e^{ik_q r}, \tag{5}$$

where $\boldsymbol{a}^*(x,z)$ and $-\boldsymbol{k}_o$ represent the complex amplitude and the wave vector of the reconstructed wave. $\boldsymbol{Q}$ and $\boldsymbol{k}_q$ are the complex amplitude and the wave vector of the first-order diffraction wave, respectively. The two-dimensional coupled-wave equations[19] can be given as

$$\begin{aligned}\cos\theta\frac{\partial a^*}{\partial x} + \sin\frac{\partial a^*}{\partial y} + ikAaQ = 0,\\ \cos\theta\frac{\partial Q}{\partial x} - \sin\frac{\partial Q}{\partial y} + ikAaa^* = 0.\end{aligned} \tag{6}$$

Similarly, the above formulas are applicable for the analysis of the photorefractive volume grating with high spatial frequency. However, k obeys the vector triangle rule, and the coupling efficiency is related to the contribution of the effective wave vector ratio in the recording process. In addition, the reconstructed intensity is limited by the effective wave vector ratio.

Taking the traditional volume grating as example to analyze the diffraction efficiency of the signal grating and the photorefractive volume grating with high spatial frequency, the diffraction efficiency η is expressed in Eqs. (7) and (8):

$$\eta(w_0) = 1 - J_0^2(w_0) - J_1^2(w_0), \tag{7}$$

$$w_0 = \frac{\pi n_1}{\lambda}\frac{\sqrt{W_R W_S}}{2\sin 2\theta}, \tag{8}$$

where $W_R = 2W_S$ is the widths of the two intersected beams $\boldsymbol{E}_r$ and $\boldsymbol{E}_o$. J_0 and J_1 are the zero and first-order Bessel functions.

Based on above analysis, the effective wave vector ratio of the photorefractive volume grating with high spatial frequency in different recording angles is shown in Fig. 2, with α taken as 50° for convenience. It increases with the

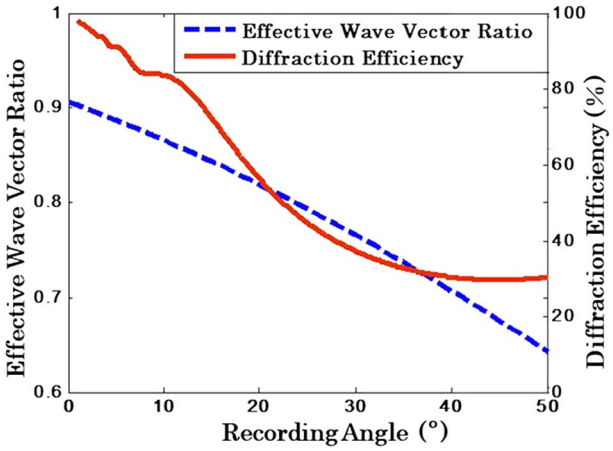

Fig. 2. Effective wave vector ratio of photorefractive volume grating with high spatial frequency and diffraction efficiency of the traditional volume grating in different recording angles.

recording angle decreasing, which indicates that the recorded modulations with high spatial frequency can be significantly improved in the small recording angle. In addition, as shown in Fig. 2, the higher diffraction efficiency can be acquired under the condition of the smaller recording angle.

In order to further verify the above analysis, three recording angles θ are chosen as 45°, 30°, and 7.5° to study the compensation effect of the modulations with high spatial frequency in the distorted wavefront in the experiment. Taking $\theta = 45°$ as an example, the experimental setup of analog OPC is depicted in Fig. 3. A 45°-cut $LiNbO_3$ crystal is used to generate the analog OPC, and the c axis is depicted by the arrow, as shown in Fig. 3. The illumination beam from a continuous laser (100 mW) with a wavelength of 532 nm is split into two by a beam splitter (BS1). The beam attenuators A1, A2 are used to adjust the two beams to the proper intensities. In the object beam "a" with the diameter of 0.75 mm, a negative United States Air Force (USAF) target is utilized for the purpose of generating a two-dimensional wide-field

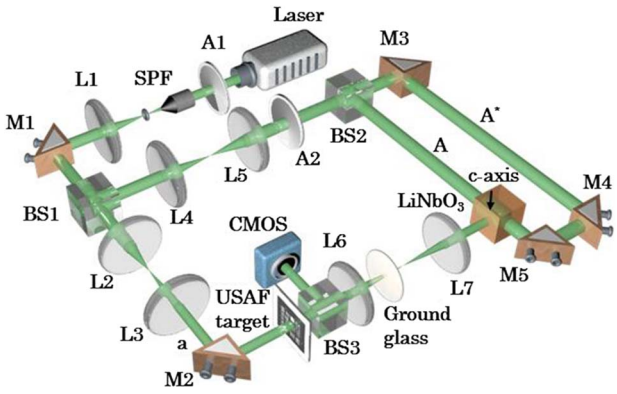

Fig. 3. Experimental setup of analog OPC. M1–M5 are reflecting mirrors, SPF represents the spatial filter, and A1, A2 are the beam attenuators. BS1–BS3 are beam splitters, and L1–L7 are the lenses. A, a, and A* represent the reference beam, the object beam, and the conjugate reference beam of A.

image pattern. A ground glass placed 5 cm behind the L2 acts as the scattering medium. The other beam of the interferometer is split further into the reference beam "A" and the conjugate reference beam "A*" by BS2 after expanding to a diameter of 15 mm. In recording, the object beam intersects with the reference beam in the crystal simultaneously for 5 min. A photorefractive volume grating with the information of the distorted wavefront is recorded in the crystal. In conjugate reconstruction, an OPC light field is generated with a conjugate reference beam to retrace the path of the original transmission. The image after OPC compensation is detected by a complementary metal–oxide–semiconductor (CMOS, Mako G-419B, pixel size 5.5 μm × 5.5 μm). The focal lengths of L2, L4, L6, L7 are 100 mm, and L1, L3, L5 are 50, 75, 150 mm, respectively. Keeping the object beam unchanging, the recording angle θ of the reference beam is varied at 30° and 7.5°, respectively, to repeat the above experiment steps.

The experimental images after OPC compensation in three recording angles and the normalized one-dimensional intensity distributions are shown in Fig. 4. Figures 4(a) and 4(b) are the images of the USAF target and the conjugate reconstructed image without the scattering medium, respectively. When the scattering medium is introduced, the random scattering inside the ground glass severely distorts the spatial phase profile and the spatial intensity distribution. The measured intensity pattern appears blurry and is filled with speckles, as shown in Fig. 4(c). The intensity distribution in the right column of Fig. 4(c) turns up as clutter and splits into multiple peaks in the rectangle area. Moreover, the maximum noise value of the background area is up to 0.95. The SNR, defined as the ratio between the maximum intensity of the rectangle area and the maximum intensity of the background area, is evaluated at approximately 1.05. Figures 4(d)–4(f) show the images after OPC compensation in the recording angles of 45°, 30°, and 7.5°, respectively. Compared with Fig. 4(b), Figs. 4(d)–4(f) show that the speckles are all reduced, and the maximum intensity of the background area decreases to 0.7, 0.48, and 0.22, respectively. Especially in Fig. 4(f), the image resolution is enhanced, and the number "5" is easy to distinguished, which indicates that the compensation effect of high spatial frequency is improved significantly in the small recording angle. The SNR corresponding to Figs. 4(d)–4(f) increases 1.4, 2, and 4.4 times that of Fig. 4(b), respectively.

Based on the three measured values of SNR, 1.43, 2.1, and 4.6, the SNR curve is fitted with the different recording angles, as shown in Fig. 5. Combining the curve of SNR and the diffraction efficiency, it is demonstrated that the high-efficiency compensation effect can be acquired by analog OPC with the smaller recording angle, which is in high consistence with the theoretical analysis.

In conclusion, we have demonstrated that the compensation effect of modulations with high spatial frequency in the distorted wavefront can be improved by optimizing the recording angle. Based on the theoretical analysis,

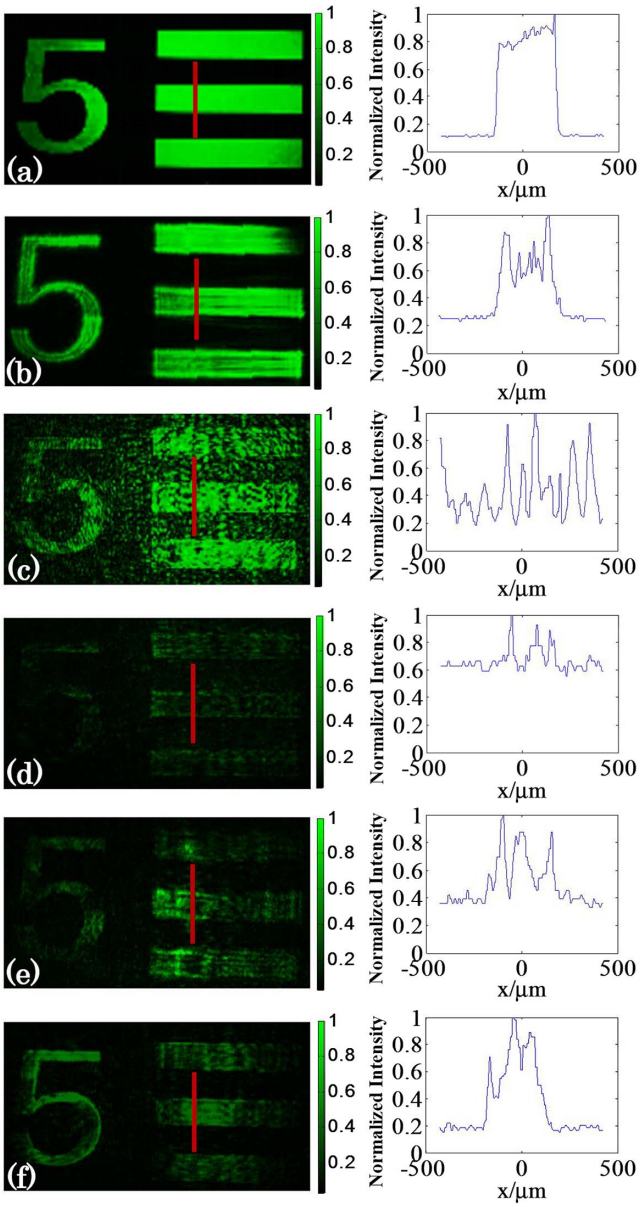

Fig. 4. Experimental results of the USAF target (left column) and normalized one-dimensional intensity distribution (right column). The horizontal axis in the right column represents the coordinate value corresponding to the length of the red line, and the middle position of the red line is 0 μm. (a) Image without ground grass. (b) Conjugate reconstructed image without ground grass. (c) Image with the ground grass. (d)–(f) Images after OPC compensation in recording angles of 45°, 30°, and 7.5°, respectively.

it is concluded that the effective wave vector ratio and the diffraction efficiency can be improved under the condition of the small recording angle. In the experiment, we choose the recording angles of 45°, 30°, and 7.5° to verify the compensation effect of high spatial frequency and to obtain the corresponding SNR. The fitted curve of the SNR is in good agreement with the theoretical diffraction efficiency. Consequently, under the condition of small recording angle, analog OPC has more efficient compensation effect on the distorted wavefront with high spatial frequency.

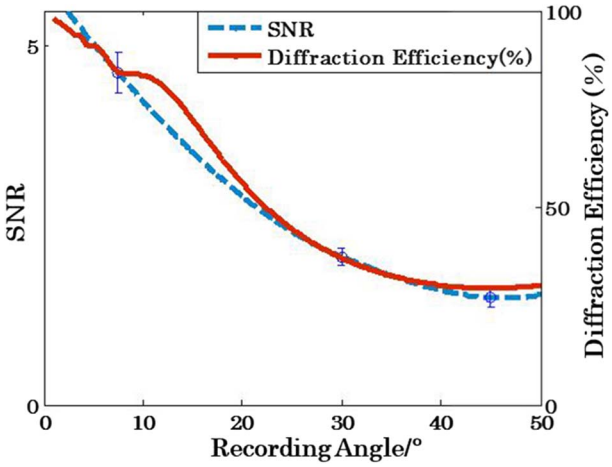

Fig. 5. Numerical fitting SNR and diffraction efficiency in different recording angles. The error bar shows the standard deviation of three experimental measurements.

We hope this work could be helpful for improving the compensation effect of analog OPC and provide a meaningful reference for optical imaging.

This work was supported by the National Natural Science Foundation of China (No. 11774364) and the Shanghai Sailing Program (No. 18YF1425900).

References

1. T. Chaigne, O. Katz, A. C. Boccara, M. Fink, E. Bossy, and S. Gigan, Nat. Photon. **8**, 58 (2014).
2. S. M. Popoff, G. Lerosey, R. Carminati, M. Fink, A. C. Boccara, and S. Gigan, Phys. Rev. Lett. **104**, 100601 (2010).
3. B. Zhuang, C. Xu, Y. Geng, G. Zhao, H. Chen, Z. He, Z. Wu, and L. Ren, Chin. Opt. Lett. **16**, 041102 (2018).
4. I. M. Vellekoop, A. Lagendijk, and A. P. Mosk, Nat. Photon. **4**, 320 (2010).
5. Y. Zhou and X. Li, IEEE Photon. J. **9**, 6100310 (2017).
6. D. Wang, E. H. Zhou, J. Brake, H. Ruan, M. Jang, and C. Yang, Optica **2**, 728 (2015).
7. Z. Yaqoob, D. Psaltis, M. S. Feld, and C. Yang, Nat. Photon. **2**, 110 (2008).
8. V. S. Sudarshanam, M. Cronin-Golomb, P. R. Hemmer, and M. S. Shahriar, Opt. Lett. **22**, 1141 (1997).
9. E. N. Leith and J. Upatneiks, J. Opt. Soc. Am. **56**, 523 (1966).
10. A. Yariv, IEEE J. Quantum Electron. **14**, 650 (1978).
11. T. R. Hillman, T. Yamauchi, W. Choi, R. R. Dasari, M. S. Feld, Y. Park, and Z. Yaqoob, Sci. Rep. **3**, 1909 (2013).
12. G. Pang, H. Liu, P. Hou, M. Qiao, and S. Han, Appl. Opt. **57**, 2675 (2018).
13. M. Cui and C. Yang, Opt. Express **18**, 3444 (2010).
14. S. Farahi, G. Montemezzani, A. A. Grabar, J. Huignard, and F. Ramaz, Opt. Lett. **35**, 1798 (2010).
15. S. C. Barden, J. A. Arns, W. S. Colburn, and J. B. Williams, Publ. Astron. Soc. Pac. **112**, 809 (2000).
16. X. Li, D. Qu, W. Wang, X. Zhao, L. Zhang, and X. Meng, Chin. Opt. Lett. **10**, 122101 (2012).
17. D. Liu, L. Liu, L. Ren, Z. Luan, and Y. Zhou, Chin. Opt. Lett. **2**, 630 (2004).
18. I. de Oliveira and J. Frejlich, J. Opt. A: Pure Appl. Opt. **5**, S428 (2003).
19. R. P. Kenan, IEEE. J. Quantum Electron. **QE-14**, 924 (1978).